University of Groningen

Synthetic and biological identities of polymeric nanoparticles influencing the cellular delivery

Rezaei, Ghassem; Daghighi, Seyed Mojtaba; Raoufi, Mohammad; Esfandyari-Manesh, Mehdi; Rahimifard, Mahban; Mobarakeh, Vahid Iranpur; Kamalzare, Sara; Ghahremani, Mohammad Hossein; Atyabi, Fatemeh; Abdollahi, Mohammad

IMPORTANT NOTE: You are advised to consult the publisher's version (publisher's PDF) if you wish to cite from it. Please check the document version below.

Document Version
Publisher's PDF, also known as Version of record

[Link to publication in University of Groningen/UMCG research database](#)

Citation for published version (APA):
Rezaei, G., Daghighi, S. M., Raoufi, M., Esfandyari-Manesh, M., Rahimifard, M., Mobarakeh, V. I., Kamalzare, S., Ghahremani, M. H., Atyabi, F., Abdollahi, M., Rezaee, F., & Dinarvand, R. (2019). Synthetic and biological identities of polymeric nanoparticles influencing the cellular delivery: An immunological link. *Journal of Colloid and Interface Science*, *556*, 476-491. https://doi.org/10.1016/j.jcis.2019.08.060
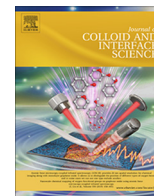
Synthetic and biological identities of polymeric nanoparticles influencing the cellular delivery: An immunological link

Ghassem Rezaei [a,b,c], Seyed Mojtaba Daghighi [d], Mohammad Raoufi [b], Mehdi Esfandyari-Manesh [b], Mahban Rahimifard [d], Vahid Iranpur Mobarakeh [e], Sara Kamalzare [e], Mohammad Hossein Ghahremani [b], Fatemeh Atyabi [b], Mohammad Abdollahi [d,f], Farhad Rezaee [g,h,*], Rassoul Dinarvand [b,*]

[a] Department of Pharmaceutical Biomaterials, Faculty of Pharmacy, Tehran University of Medical Sciences, Tehran, Iran
[b] Nanotechnology Research Center, Faculty of Pharmacy, Tehran University of Medical Sciences, Tehran 1417614411, Iran
[c] Medical Biomaterials Research Center (MBRC), Tehran University of Medical Sciences, Tehran, Iran
[d] Pharmaceutical Sciences Research Center, The Institute of Pharmaceutical Sciences (TIPS), Tehran University of Medical Sciences, Tehran, Iran
[e] Department of Hepatitis and HIV, Pasteur Institute of Iran, Tehran, IR, Iran
[f] Department of Toxicology and Pharmacology, Faculty of Pharmacy, Tehran University of Medical Sciences, Tehran, Iran
[g] Department of Gastroenterology-Hepatology, Erasmus Medical Center, Rotterdam, the Netherlands
[h] Department of Cell Biology, University Medical Center Groningen, University of Groningen, Groningen, the Netherlands

GRAPHICAL ABSTRACT
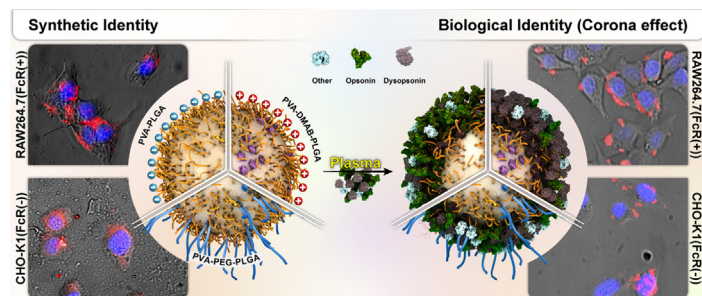
ARTICLE INFO

ABSTRACT

Enhanced understanding of bio-nano interaction requires recognition of hidden factors such as protein corona, a layer of adsorbed protein around nano-systems. This study compares the biological identity and fingerprint profile of adsorbed proteins on PLGA-based nanoparticles through nano-liquid chromatography-tandem mass spectrometry. The total proteins identified in the corona of nanoparticles (NPs) with different in size, charge and compositions were classified based on molecular mass, isoelectric point and protein function. A higher abundance of complement proteins was observed in modified NPs with an increased size, while NPs with a positive surface charge exhibited the minimum adsorption for immunoglobulin proteins. A correlation of dysopsonin/opsonin ratio was found with cellular uptake of NPs exposed to two positive and negative Fc receptor cell lines. Although the higher abundance of dysopsonins such as apolipoproteins may cover the active sites of opsonins causing a lower uptake,

Cellular uptake
Delivery

the correlation of adsorbed dysopsonin/opsonin proteins on the NPs surface has an opposite trend with the intensity of cell uptake. Despite the reduced uptake of corona-coated NPs in comparison with pristine NPs, the dysopsonin/opsonin ratio controlled by the physicochemistry properties of NPs could potentially be used to tune up the cellular delivery of polymeric NPs.

1. Introduction

Polymeric drug delivery systems are promising carriers that provide efficacious approaches to improve the delivery of active pharmaceutical ingredients and alleviate the toxicity of pharmaceutical payloads through passive and active targeting methods [1–5]. Poly (D, L lactide-co-glycolide) (PLGA) is one of the most widely used biodegradable synthetic polymers for drug delivery [1,6]. The PLGA-based NPs have been successfully used in many therapeutic and diagnostic products in the forms of implants, encapsulated macromolecules (proteins, peptides, and genes) and chemotherapeutic agents [7,8].

The interaction between proteins in plasma, serum, cerebrospinal fluid, synovial fluid and vitreous [9] with NPs, reduces the NPs surface energy and enhances the total entropy of the proteins [10,11]. This phenomenon is known as protein corona, which is distinct from the pristine NP, containing biomolecules such as sugars, lipids and proteins [12–19]. The dynamic nature of corona shell consists of loosely proteins with low-affinity (soft corona) [20,21] replaced by high-affinity proteins (hard corona) over time [10,15,22]. The key determining factors for the NPs uptake is the interaction of particles with the cell membrane, which can be controlled by the biological identity, physicochemical properties (such as size and shape) as well as surface chemistry of NPs [23,24]. In addition to the shape and size, dimensions of nano-systems such as 2D-nanosheets could also affect intracellular process associated with bio-nano interaction and its cellular uptake [25,26]. The protein corona composition of NPs plays an important key role on the fate of the in-vivo and in-vitro bio-nano interface outcomes [27]. The control of synthetic identity and surface chemistry modification of NPs orchestrates the fate of NPs in drug delivery [8]. Therefore, recognizing the influence of NPs physicochemical factors on NPs biological identities would accelerate the progress of NPs application towards clinical applications [28–34]. The modification of PLGA NPs surface by cationic polymers and stabilizer such as didodecyldimethylammonium bromide (DMAB) or by polymers with antifouling and hydrophilic properties (e.g. polyethylene glycol (PEG) and polyvinyl alcohol (PVA)) could encourage the interaction of NPs with the cell membrane and the residence time of drug in bloodstream respectively [35–37]. The interaction of the positive charge of the DMAB-coated NPs with the negative surface of the cell membrane promises a higher uptake than with negative charge NPs [38].

Opsonization as a process of biological system against exogenous agents is part of the corona formation which may affect the biological identity and the in-vivo fate of NPs. Opsonins such as complement proteins, fibrinogen and immunoglobulins are considered as the most abundant protein corona. Removal of NPs by the immune system occurs by the Fc-receptors on phagocytic cells via binding to the opsonins adsorbed on the surface of NPs. On the other hand, albumin and apolipoproteins known as dysopsonins significantly affect the biological distribution of NPs and their uptake via cell membranes [39]. The hydrophilic polymers such as PVA and PEG have been employed around the NPs in order to manage the opsonization process [22]. The adsorption of albumin, fibrinogen, and immunoglobulins has also been identified at the

hydrophilic surface of NPs [40]. In addition to the hydrophilic properties of NPs, increased adsorption of proteins occurs by increasing the size of NPs which is associated with the NPs curvature. On the other hand, the positive surface charge is related to an increase in the amount of adsorbed proteins as compared to the negative charge [41,42]. As with the NPs surface charge, covering the active sites of target agents by protein corona, NP surface chemistry may also control the adsorption of specific proteins in the corona shell. This approach has been used through intriguing selective targets based on surface chemistry in cellular and in-vivo investigations [43–46].

Among the different types of cells, the interaction of NPs with macrophages is important due to the role of macrophages in the clearance efficiency of NPs [47]. The intensification of the interaction between corona-coated NPs and the receptor of the target cells could be controlled by peculiar proteins adsorbed from various functional groups of the plasma proteins [48].

In this current study, the contribution of three factors; including size, composition, and surface charge to the corona profile was investigated in PLGA-based NPs. To this end, protein corona fingerprint of NPs with different surface coatings, unique/similar/common proteins, protein fractions with higher and lower abundance than 1% on the corona, the ratio of dysopsonins/opsonins in association with NPs uptake in two positive and negative FcR cell lines [49] were determined using nLC-MS/MS.

2. Materials and methods

2.1. Materials and reagents

The PLGA copolymer with a free carboxylic acid (LA/GA = 50:50 M ratio Resomer RG 502H, weight average MW:12,000 g/mol) was obtained from Boehringer-Ingelheim (Ingelheim, Germany). Poly (ethylene glycol) (PEG)- bis-amine [NH2–PEG–NH2] (weight average MW: 3350 g/mol), N,N′-Dicyclo hexylcarbodiimide (DCC), sulfo-N-hydroxysuccinimide (NHS), Polyvinyl alcohol (PVA) (weight average MW: 9000–10,000 g/mol) and Didodecyldimethylammonium bromide (DMAB) were purchased from Sigma Aldrich (St. Louise, MO, USA). Nile red with 99% purity was obtained from ACROS Organic (Geel–Belgium). Enzymatic agents for protein digestion-dithiothreitol (DTT) and trypsin (proteomics grade) were purchased from sigma Aldrich (St. Louise, MO, USA). Ethyl acetate and acetone with purity of 99.5% were purchased from Merck (Darmstadt, Germany). LC-MS grade acetonitrile and formic acid were obtained from Fisher Scientific (Ottawa, ON, Canada). High quality water (Millipore, USA) was used throughout the experiment. All other utilized materials and analytical grade chemicals were purchased from Sigma Aldrich (St. Louise, MO, USA) without further purification.

2.2. Human plasma and cell culture materials

Normal human plasma (blood group B+) was obtained from blood transfusion organization (Tehran, Iran). All procedures regarding use of human plasma were in accordance with the

ethical approval of research committee of Tehran University of Medical Sciences (#93-01-33-24870). The plasma samples were divided into 5 ml cryovials to prevent the re-thawing and re-freezing of the plasma. Chinese Hamster Ovary (CHO)-K1 (C645) and murine macrophages RAW 264.7 (C639) cell lines were obtained from the Pasteur Institute of Iran (Tehran, Iran). Dulbecco's modified Eagle's medium (DMEM), Opti-MEM medium, fetal bovine serum (FBS) and trypsin-EDTA were purchased from Thermo Fisher Scientific (Gibco, USA).

2.3. Synthesis of NPs with modified surfaces

2.3.1. PVA-modified PLGA NP (PVA-PLGA)

All NPs were prepared in two ranges of size. The synthesis of PVA-PLGA NPs was performed according to the previous modified nanoprecipitation method [50]; the PLGA polymer (LA/GA = 50:50 M ratio Resomer RG 502H, MW:12,000 g/mol) and the Nile red 99% (Acros organic, Geel, Belgium). As indicated in Table 1, they were dissolved in a proper organic solvent and injected dropwise in to a defined volume of the diffusing phase containing PVA (MW: 9000–10,000 g/mol) through a needle syringe under magnetic stirring (Heidolph, Germany). After evaporation of the solvent and size stabilization, the formed NPs were centrifuged three times at 24,000g for 15 min and resuspended in milli-Q grade water (TKA, Genpure) and stored at 4 °C.

2.3.2. PVA-modified DMAB-PLGA NP (PVA-D-PLGA)

PVA-D-PLGA NPs were synthesized by a modifying emulsification-diffusion methods [35,38,51]. Briefly, as shown in Table 1, the polymer PLGA and Nile red was dissolved in 2 ml ethyl acetate. The ethyl acetate solvent phase was poured into a 6 ml non-solvent containing 5–6.67 mg/mL DMAB. It was followed by emulsification using an adjustable high-speed emulsifying homogenizer (IKA T18 Ultra-Turrax®) at 16,000 rpm for 8 min. Then, it was slowly added into 14 ml diffusing phase containing PVA at mentioned amounts and stirred overnight at 850 rpm to remove the solvent. The stabilized NPs were rinsed with milli-Q grade water (ultrapure grade water) and centrifuged three times (24,000g, 15 min) and finally stored at 4 °C.

2.3.3. PEG–PLGA-NH2 conjugate

Initially and in order to prepare the PVA-modified PEG-PLGA NPs (PVA-PEG-PLGA), the PLGA copolymer was converted to amine-capped diblock copolymer by PEG. PLGA–PEG–NH2 diblock conjugate was synthesized according to the previously mod-

ified method [52,53]. Briefly, PLGA (0.1494 mmol) was dissolved in 8 ml dichloromethane (DCM) as the minimum volume and then carboxyl end-capped group was activated by 1.494 mmol dicyclohexylcarbodiimide (DCC) and same mmol of N-Hydroxysuccinimide (NHS) at room temperature under nitrogen umbrella for 24 h. Activated PLGA (0.083 mmol) was dissolved in 8 ml DCM and then added slowly to 100 mg PEG–bis-amine (weight average MW: 3350 g/mol) which was previously dissolved in 2 ml methylene chloride in a dropwise manner. The reaction was carried out for 12 h under the nitrogen atmosphere (PLGA/PEG–bis-amine stoichiometric molar ratio:1/5) and the resultant solution was precipitated by adding ice-cold diethyl ether. The obtained amine-capped di-block copolymer PLGA-PEG-NH2 was filtered and dried using vacuum.

2.3.4. PVA-modified PLGA-PEG NP (PVA-PEG-PLGA)

PVA-PEG-PLGA NPs were fabricated by nanoprecipitation or so-called solvent displacement method. Briefly, the PEG-PLGA di-block copolymer with amine end-capped group and the Nile red was dissolved in acetone and then injected dropwise to a defined volume (Table 1) of the diffusing phase containing PVA via a needle syringe under magnetic stirring [54]. After evaporation of the acetone and stabilization of the NP sizes, the pegylated NPs were centrifuged three times (16,000g, 15 min), washed, resuspended and stored at 4 °C.

2.4. Characterization of synthesized NPs

NPs size (z-average), particle size distribution and the surface charge of different NPs were measured by dynamic light scattering (DLS) (Malvern Zetasizer ZS, Malvern, UK) at room temperature. In addition, surface morphology and size analysis in dry state were measured by the Scanning Electron Microscopy (SEM) method while the morphology of NPs core-shell was captured through Transmission Electron Microscopy (TEM) (CM30, Philips). For microscopic imaging, fresh nanosuspension was dropped into a coverslip and dried at room temperature. Subsequently, the coverslip was sputtered with gold under vacuum conditions where the morphology and size analysis were investigated by the MIRA\\TESCAN instrument through energy of 7KV, the working distance of 7 mm and at 40–50kx magnification.

In order to provide further structural characterization of the di-block copolymer, the ¹H NMR spectroscopy (Brucker 500 MHz) investigation was carried out. For determining the amount of PEG in the copolymer and outside shell, the protons of PEG (CH2,

Table 1
List of materials and preparation methods of various PLGA-based NPs.

Nickname	PVA-PLGA < 150 nm	PVA-PLGA > 150 nm	PVA-D-PLGA < 150 nm	PVA-D-PLGA > 150 nm	PVA-PEG-PLGA < 150 nm	PVA-PEG-PLGA > 150 nm
Type of NPs	PVA-modified PLGA		PVA-modified DMAB-PLGA		PVA-modified PLGA-PEG	
Size ranges (nm)	<150	>150–250	<150	>150–250	<150	>150–250
Preparation method	Nanoprecipitation		Emulsion diffusion		Nanoprecipitation	
List of materials						
PLGA 502H (mg)	30	50	40	60	–	–
PEG-PLGA (mg)	–	–	–	–	30	30
Polyvinyl alcohol (mg)	20	30	20	30	15	15
Acetone (ml)	4.850	1	–	–	3	1.5
Dichloromethane (µl)	150	–	–	–	–	–
Ethyl acetate (ml)	–	–	2	2	–	–
DMAB (mg)	–	–	40	30	–	–
Nile Red (% of polymer content)				0.5		
Purified water (ml)	20	40	20	20	25	25
Stirring speed (rpm)	1000	600	–	–	800	600
Homogenizer speed (rpm)	–	–	16,000	16,000	–	–

3.6 ppm) were quantitatively compared to either the protons of the lactic (CH, 1.5 or CH3, 5.2 ppm) or glycolic units (CH2, 4.8 ppm) while considering the molecular weight of each unit. Also, the PEG percentage in the copolymer was defined by the length of each copolymer block.

2.5. Protein corona analysis

In order to identify the proteins present on NPs (Table 1), the total amount of each NP was adjusted to 200 μg in a specific volume (μL). All types of NPs were centrifuged at 6000g for 10 min. After removal of supernatant, the pellets were resuspended in 300 μL water after which 300 μL plasma was added to each pellet, mixed gently and incubated for 2 h at room temperature. Next, the obtained samples were centrifuged for 20 min at 12,500g and the pellets were washed three times with water to remove free plasma. Next, the pellets were resuspended in 100 μL water containing 2% formic acid and 1 μg trypsin and incubated at 37 °C for 24 h; during the incubation time, the samples were mixed several times by vortexing. After centrifugation at 12,500g for 60 min, the peptides were collected and reduced by 15 μL 1% dithiothreitol (DTT) and dried in a speed-vacuum. Finally, the peptides were resuspended in 20 μL water containing 2% formic acid, where 2 μL of each NPs-corona derived peptides fraction was injected into nLC-MS/MS (Q-Exactive-plus, Thermo fisher).

2.6. Data analysis

Raw mass spectrometry data were analyzed using Peaks version 8.5 (bioinformatics Solutions Inc., Waterloo, Ontario, Canada) with a False Discovery Rate (FDR) of 0.1%. Precursor and fragment ions tolerance were 10 ppm and 0.02 Da, respectively. Trypsin with non-specific cleavage on one end of the peptide was allowed. Carbamidomethylation of cysteine residues was considered as fixed modification while oxidation of methionine was regarded as a variable modification. The human SwissProt database contained 20,195 entries.

After data analysis, result visualization, validation and, filtration by peaks bioinformatics software provides the final report. The final report included the molecular weight, spectral count and other data of proteins that have been identified. For protein semi-quantitative analysis, the following formula was used. The relative protein abundance of protein k (RPA_k) in the protein shell is the normalized percentage of the spectral count which is equal to the following equation [55,56]. SpC is the spectral count identified, and Mw is the molecular weight (kDa) of protein k. n represents the number of proteins identified in the protein corona. The SpC of each identified protein was normalized to total SpC belonging to all proteins identified for covered NPs surfaces. RPA_k expresses the percentage of each protein in the total protein mass.

$$RPA_{k=}N_P S_P C_k = \left(\frac{(S_p C/(M_w)_k)}{\sum_{t=1}^{n} (S_p C/(M_w)_t)} \right) \times 100$$

2.7. Cellular uptake of NPs

The CHO-K1 and RAW 264.7 cells were expanded in DMEM supplemented with 10% FBS, 100 U/mL penicillin, and 100 μg mL^{-1} streptomycin at 37 °C under a humidified atmosphere of 5% CO2. The cellular uptake of NPs was investigated using FACS flow cytometer (Mindray, China) and Confocal Laser Scanning Microscopy (CLSM, Nikon Inc., Switzerland).

Briefly and in order to evaluate the cellular uptake of pristine and corona-coated NPs, CHO-K1 and RAW 264.7 cells were independently cultured in 6-well plates at a density of 1×10^5 cells

per well for 24 h. They were then washed and treated with Nile red-labeled NPs (pristine and corona-coated NPs) in serum-free media (Opti-MEM) for 4 h at 37 °C. NPs were first incubated with human plasma, and then centrifuged and washed to remove unbounded proteins. Pristine and corona-coated NPs were resuspended in serum free medium, and both cell lines were separately incubated with NPs at the final concentration of 500 μg mL^{-1}. After incubation time, the cells were rinsed with Phosphate Buffered Saline (PBS), detached from culture plate using trypsin-EDTA solution and finally the fluorescence intensity of cells was quantitated using FACS flow cytometer at 488 nm excitation and 585/40 band-pass (FL2) filter. Data interpretation was performed using FlowJo® v10 software. FSC versus SSC gating was used to remove cell debris, and the fluorescent histogram parameters were determined from this gated scatter region [57].

Also, CHO-K1 and RAW 264.7 cells were cultured in 8-well cell culture-treated chamber slides (SPL, Korea) at a density of 1×10^4 cells per well for 24 h, and then washed by PBS and treated with Nile red-labeled PLGA-based NPs (pristine and corona-coated NPs) in serum-free media (Opti-MEM) for 4 h at 37 °C. After incubation, the cells were washed with PBS, fixed in paraformaldehyde (4% in PBS) for 10 min, stained with 2 μg mL^{-1} DAPI (Invitrogen) and finally inspected using CLSM. The fluorescence localization images of the pristine and corona-coated NPs in the cells were captured with a 40x oil immersion objective lens. Nile red-loaded PLGA-based NPs were excited and detected at 552 and 636 nm, respectively.

3. Results

3.1. Nps characterization

NPs with various compositions and surface charges were synthesized within a size range of less than 150 nm and larger than 150 up to 250 nm. NPs characterization results are presented in Table 2 and ESI, Figs. S1, S2. Considering that the final surface of all NPs was modified with PVA, it was observed that only PVA-D-PLGA NPs were positively charged mainly due to the use of DMAB inducing positive charge. However, the core of NPs in other groups (PVA-PLGA, PVA-PEG-PLGA) had negative and slightly negative charges because of the presence of carboxylic acid end caps. The acidic end terminal conjugation of PLGA copolymer by the bis amine- polyethylene glycol resulted in slightly negative charge of the PVA-PEG-PLGA NPs because of the shielding effect of the PEG chain where the NH2-PEG grafting to the PLGA copolymer was confirmed by the NMR spectrum (ESI, Fig. S3). According to the ^{1}H NMR spectra, the ratio of PEG to PLGA was measured as 1:1. The PEGylation percentage of PEG-PLGA di-block copolymer was calculated as 21.8 wt%.

3.2. Quantitative evaluation of protein corona on PLGA-based NPs

3.2.1. Classification of detected proteins based on common, similar and unique proteins

After incubation of PLGA NPs with blood plasma, the number and percentage of high abundance adsorbed proteins detected on the surface of polymeric NPs are reported in Table 3. In this table, the proteins with a High Relative Abundance of 1% ($RPA > 1\%$) were sorted in a descending order (ESI, Table S1 and Fig. S4). A comparison of the type and amount of proteins higher than 1% considering molecular weight and the percentage of RPA has been presented in Fig. 1.

In this study, common proteins [44] refers to the adsorbed proteins with a high abundance of 1% in the corona while similar proteins represent proteins detected at higher and lower than 1%

Table 2
Z-average (hydrodynamic diameter, nm), zeta-potential, size distribution (polydispersity index, PDI) and synthesis methods of the synthesized PLGA-based NPs (pristine NPs).

Nickname	PVA-PLGA < 150 nm	PVA-PLGA > 150 nm	PVA-D-PLGA < 150 nm	PVA-D-PLGA > 150 nm	PVA-PEG-PLGA < 150 nm	PVA-PEG-PLGA > 150 nm
Type of NPs	PVA-modified PLGA		PVA-modified DMAB-PLGA		PVA-modified PLGA-PEG	
Size ranges (nm)	<150	>150–250	<150	>150–250	<150	>150–250
Z-average of size (nm) ± SD	122 ± 2	184 ± 1	123 ± 3	197 ± 1	99 ± 2	186 ± 1
PDI ± SD	0.191 ± 0.02	0.122 ± 0.03	0.241 ± 0.01	0.197 ± 0.03	0.187 ± 0.02	0.096 ± 0.01
Zeta potential (mV) ± SD	Negative −17.9 ± 0.5	Negative −16.3 ± 1.0	Positive +16.5 ± 0.7	Positive +23.1 ± 1.0	Neutral to slightly negative −8.3 ± 1	Neutral to slightly negative −8.6 ± 1.5
Total Surface area (cm^2/µg)	0.48	0.27	0.71	0.27	0.55	0.24
Composition	PLGA-COOH + PVA	PLGA-COOH + PVA	PLGA-COOH + DMAB (PVA modified)	PLGA-COOH + DMAB (PVA modified)	PLGA-PEG-NH2 (PVA modified)	PLGA-PEG-NH2 (PVA modified)
Synthesis method	Nanoprecipitation		Emulsion Diffusion		Nanoprecipitation	

Table 3
Number and percentage of proteins identified on corona coated PLGA-based NPs surfaces and the unique protein characterizations.

Nickname	PVA-PLGA < 150 nm	PVA-PLGA > 150 nm	PVA-D-PLGA < 150 nm	PVA-D-PLGA > 150 nm	PVA-PEG-PLGA < 150 nm	PVA-PEG-PLGA > 150 nm
No. of detected protein	187	220	197	196	179	191
Z-average of size (nm) ± SD	179 ± 3	283 ± 2	189 ± 2	298 ± 1	164 ± 3	266 ± 2
Zeta potential (mV) ± SD	−9.86 ± 0.5	−8.4 ± 1.0	−2.0 ± 0.7	−2.9 ± 0.4	−3.9 ± 1.0	−4.8 ± 0.8
No. and percentage of protein abundance (*RPA* > 1%)	26; 64.02%	25; 58.80%	25; 64.55%	26; 63.93%	23; 62.72%	25; 64.57%
No. and percentage of protein abundance (*RPA* < 1%)	161; 35.98%	195; 41.20%	172; 35.45%	170; 36.07%	156; 37.28%	166; 35.43%
No. of Similar protein	132					
No. of unique protein	5	20	33	2	9	14
Abundance percentage of unique protein (%)	2.270	1.193	1.427	0.159	0.919	1.305
The physiological groups of unique proteins.	Tissue Leakage Immunoglobulins	Tissue Leakage Immunoglobulins	Tissue Leakage Complement system Lipoproteins coagulations	Tissue Leakage Complement system	Tissue Leakage Immunoglobulins	Tissue Leakage Immunoglobulins
Mw (kDa.) of unique protein	100–200 10–100	>500 100–200 10–100	>500 200–300 100–200 10–100	80–100 30–40	10–70	>500 100–200 10–70

abundance. Further, *Unique* proteins [44] refer to the proteins that could only be detected on the surface of a specific NP. Venn diagram analysis of NPs in different groups identified 132 similar proteins in all formulations (Fig. 2), while the maximum number and relative abundance of unique proteins were detected on the surface of PVA-D-PLGA and PVA-PLGA NPs with the size of less than 150 nm respectively (Fig. 3a, b and ESI, S5). The characterization of *unique* proteins adsorbed on the surface of NPs is reported in Table 3. Concerning physiological groups, *unique* proteins detected on the surface of PVA-PLGA and PVA-PEG-PLGA NPs were found to belong to the immunoglobulins where unique proteins were associated with tissue leakage proteins in all NPs (Table 3).

3.2.2. Classification of detected proteins based on molecular mass and isoelectric point

Fig. 3c displays the molecular mass of adsorbed proteins of which approximately 90% of the proteins are composed of proteins under 100 kDa molecular weight. Percentage changes of *RPA* in regions 10–20 and 60–70 kDa were compared in groups of PVA-PLGA, PVA-D-PLGA, PVA-PEG-PLGA NPs. Accordingly, the maximum abundance of 60–70 and 10–20 kDa proteins was associated with the positively charged PVA-D-PLGA and PVA-PLGA NPs, respectively. The greatest abundance of proteins within the range of 10–20 kDa is related to the immunoglobulins where the main protein within the range of 60–70 kDa is albumin.

The isoelectric point of proteins adsorbed on the surface of NPs is presented in Fig. 3d. Percentage changes of *RPA* in the isoelectric point regions of 5–6 and 8–9 were significantly altered as compared to the other isoelectric points for all NPs. In addition, representative *RPA* results of isoelectric point analysis of adsorbed protein groups are exhibited in ESI, Fig. S6. The abundance of immunoglobulins on the surface of PVA-D-PLGA in the isoelectric point regions of 5–6 and 8–10 was lower than on the rest of NPs; complement system proteins showed a comparable change in the proteins abundance with an isoelectric point of 6–8 (ESI, Fig. S6b). Significant changes in the proteins abundance of albumin and lipoproteins were associated with the isoelectric point of 5–6 and 5–7 respectively (ESI, Fig. S6c, d).

3.2.3. The classification of adsorbed proteins based on function

The total percentage of protein abundance ($\sum RPA > 1\%$ or $\sum RPA < 1\%$) was determined for all detected proteins, classified into several functional groups and depicted in Fig. 4. Although the high percentages of detected complement proteins are found to be related to the protein with lower than 1% abundance, significant changes have been identified in abundances higher than of 1% complement proteins. As displayed in Fig. 4a and b, the lowest and highest abundance of complement proteins with *RPA* > 1% was associated with PVA-PEG-PLGA and PVA-D-PLGA NPs, respectively. In contrast to PVA-PLGA, the percentage of proteins in coagulation
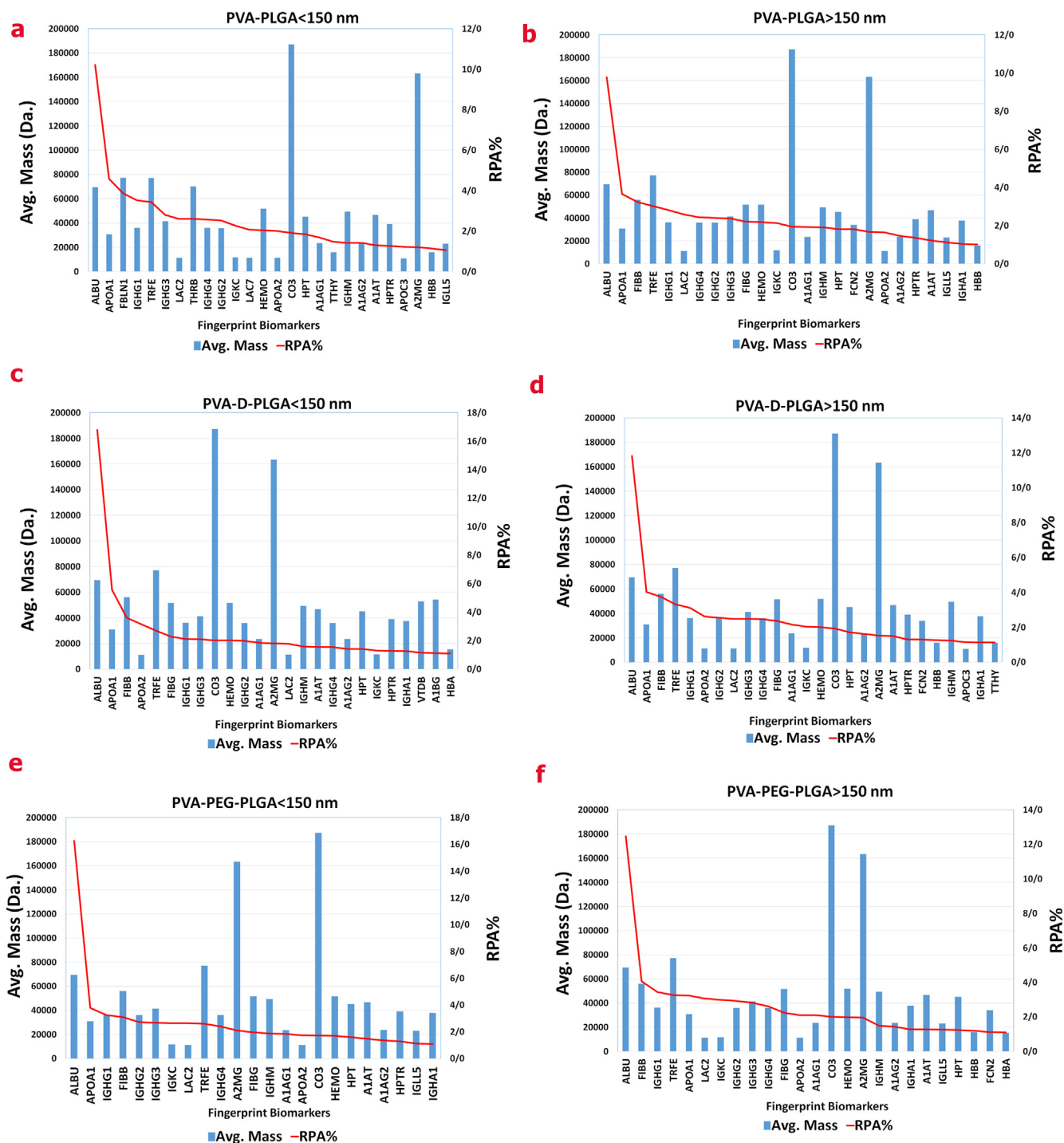
Fig. 1. *RPA* and average mass of most abundant proteins (*RPA* > 1%) on NPs with a small size (a, c, e) and mid-size (b, d, f).

cascades with *RPA* < 1% increase in other NPs (Fig. 4c and d). Abundance of immunoglobulins in PVA-D-PLGA has been less than in other NPs where the ratio of $\sum RPA$ > 1% to $\sum RPA$ < 1% was 1.5–2 folds (Fig. 4e and f). Consistent with positively charged PVA-D-PLGA NPs, the percentages of immunoglobulins adsorbed on the PVA-PLGA and PVA-PEG-PLGA NPs surface were detected as the most abundant protein in the corona mixture. The PVA-D-PLGA NPs exhibited a slightly higher adsorption of acute phase proteins compared to either PVA-PLGA or PVA-PEG-PLGA (Fig. 4g, h). Unlike acute phase proteins, tissue leakage proteins were the only protein group not representing *RPA* > 1% and it varied within 3% <*RPA* < 9% (Fig. 4I and j). The results of plasma proteins called the other

plasma components are shown in Fig. 4k and l. The *RPA*% of this group was calculated as 21 < *RPA*% < 30 for the various NPs where more albumin was adsorbed to the surface of positively charged PVA-PLGA and PVA-D-PLGA NPs. The *RPA* for lipoproteins group of corona was measured as 7.5 < *RPA*% < 13 (Fig. 4m and n).

3.2.4. Classification of adsorbed proteins based on NP size, charge and composition

The relative abundance of common proteins (*RPA*% > 1) for each group of NPs with a size range of less than 150–250 nm is reported in Fig. 5a.
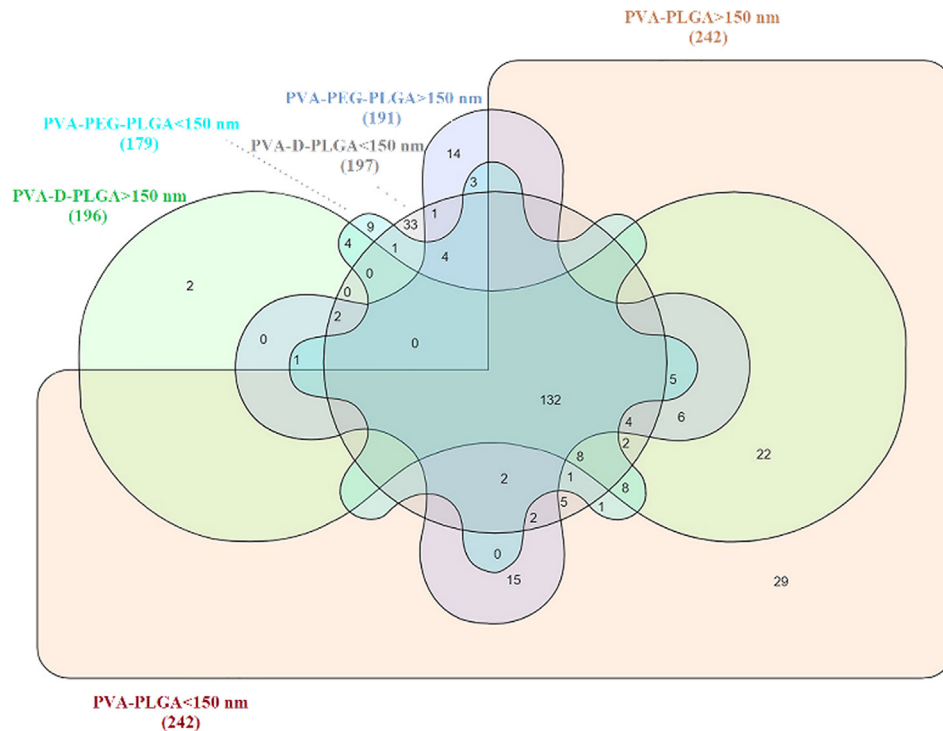
Fig. 2. Venn diagram reporting the number of *unique* and *similar* proteins identified on the PLGA-based NPs.

Increasing PVA-PLGA NPs size has led to raised *RPA* of the complement and acute phase proteins while other protein groups such as lipoproteins, immunoglobulins and etc. indicated a descending trend. However, the results of *RPA* of PVA-ᴅ-PLGA NPs due to the positive surface charge revealed an ascending trend in the complement, immunoglobulins, acute phase and the coagulation proteins while the rest of protein groups showed a falling trend. In PVA-PEG-PLGA, due to the increased size and slightly negative surface charge, *RPA* changes showed a growing trend at complement proteins, immunoglobulins and coagulation proteins. Interestingly, complement proteins revealed a rising *RPA* trend associated with the increasing size in all NPs, while the relative abundance of lipoproteins and albumin decreased concurrent with size enlargement. In Fig. S5(ESI), the number of unique and similar proteins were affected by the size of NPs. The number of unique proteins in PVA-ᴅ-PLGA NPs under 150 nm is more remarkable than the large size range of same NPs. The size-dependent discrepancy of the numerical and relative abundance of unique proteins are illustrated in Fig. 3a, b. In small-sized PLGA NPs, the relative abundance of complement system proteins under 1% was less than the mid-sized NPs, while the abundance of adsorbed complement protein greater than one percent had an increasing trend compared to mid-sized NPs. The effects of surface charge on protein corona profile in PVA-PLGA and PVA-ᴅ-PLGA NPs are shown in (ESI, Fig. S7a). A notable point in this case is that in the midsized range of NPs with a positive charge, the relative abundance of adsorbed opsonins (complement proteins and immunoglobulins) and dysopsonins were reduced and augmented, respectively. Further, the adsorption of acute phase proteins was enhanced by shifting the surface charge from negative to positive by 3.5% for midsized NPs. On the other hand, comparing the midsized range of NPs with less than 150 nm, the percentages of complement and coagulation proteins were found to have an opposite trend by shifting the negative to positive surface charge (ESI, Fig. S7-a). The effect of NP composition on the protein corona is presented in (ESI, Fig. S7-b). By modifying the composition of the copolymer from PLGA to

PEG-PLGA, in both size ranges, the quantity of complement proteins decreased, while the relative abundance of dysopsonins (albumin) increased significantly. In NPs with the size less than 150 nm the modification of copolymer from carboxyl end-capped PLGA to Pegylated PLGA revealed a significant reduction in the adsorption of immunoglobulins, coagulation, and lipoproteins where the trend of adsorbed proteins of midsized NPs was reversed.

3.3. Dysopsonins/opsonins ratio

The major part of 10–20 kDa (immunoglobulins) and 60–70 kDa proteins (albumin) were opsonins and dysopsonins groups respectively. According to the molecular mass of the adsorbed proteins on the surface of NPs, there was a significant difference in two regions of 10–20 kDa and 60–70 kDa with respect to *RPA* of albumin and immunoglobulins (Fig. 3c). The proportion of *RPA* for this groups is considered as the ratio, which is larger than one due to the high relative abundance of dysopsonins (Fig. 5b). Fig. S8-a (ESI), displays the abundance of apolipoproteins and other plasma components where the abundance variation of other plasma components greater than to less than 1% deviates from 3 to 10-fold for all NPs. Although the PVA-ᴅ-PLGA has adsorbed a high content of the lipoprotein amounts above 1%, the PVA-PLGA and PVA-ᴅ-PLGA NPs dominated the maximum and minimum abundance above 1% of adsorbed other plasma components respectively. In Fig. S8-b (ESI), the abundance of greater and less than 1% of the complements and immunoglobulin protein for all NPs is shown while the percentage of immunoglobulins adsorbed on the surface of PVA-ᴅ-PLGA is the lowest compared to other NPs. Fig. 6 summarizes the relative abundance of opsonins and dysopsonins adsorbed on NP surfaces. In NPs less than 150 nm, the ratio of dysopsonins/opsonins was as PVA-ᴅ-PLGA > PVA-PEG-PLGA > PVA-PLGA. On the other hand, when the NP size was more than 150 nm, the ratio was equal to PVA-ᴅ-PLGA > PVA-PEG-PLGA > PVA-PLGA.
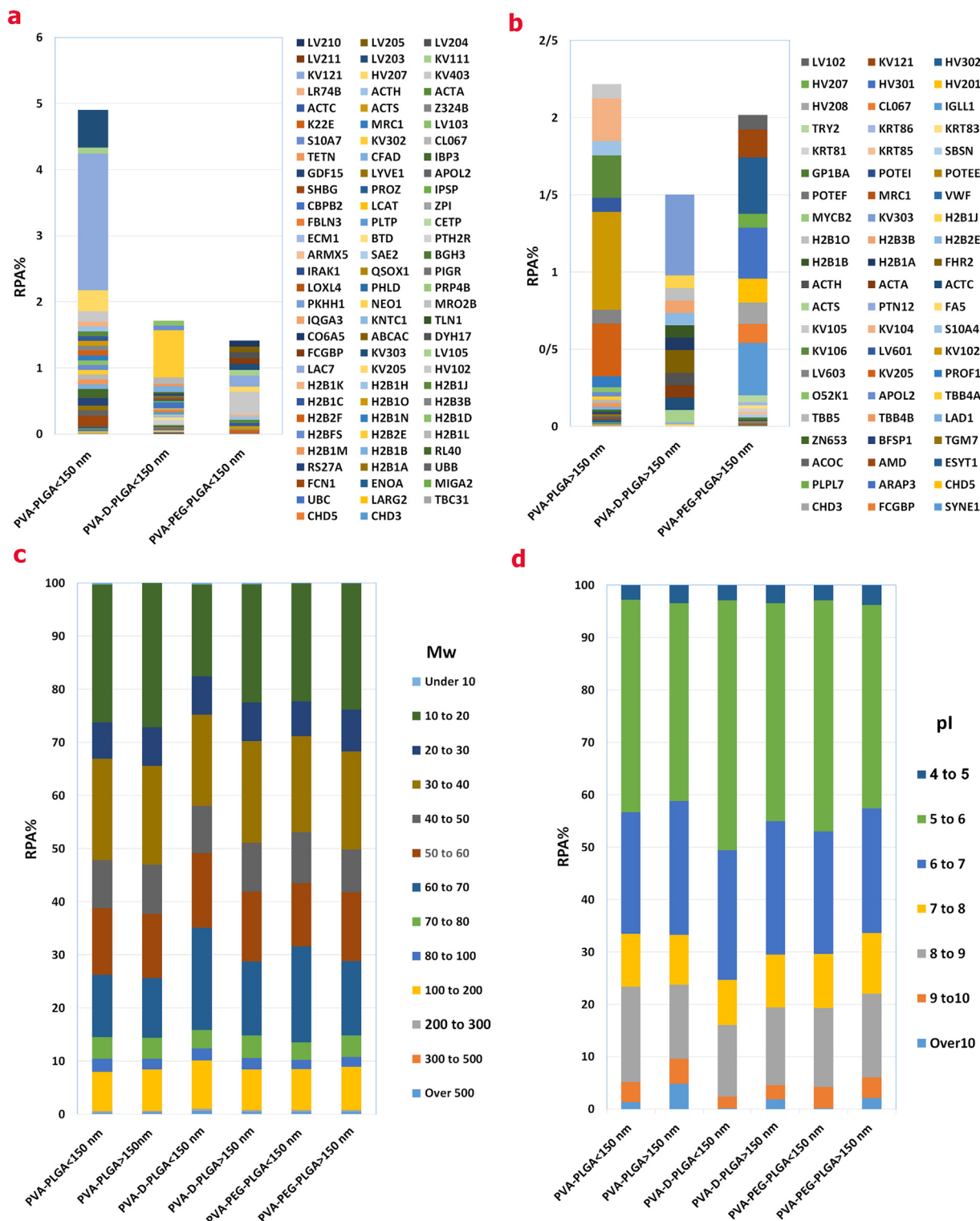
Fig. 3. *Unique* proteins in PLGA-based NPs in two size ranges of less than 150 nm (a) and larger than 150 nm (b); *RPA* of corona proteins classified according to their molecular mass (c) and isoelectric point (d).

3.4. Cellular uptake of pristine and corona coated NPs

Cellular uptake of NPs was assessed in two cell lines, RAW264.7 and CHO-K1 which are FcR+ and FcR- respectively as shown in Fig. 7a, b and S10 (ESI). The results reveal that the cellular uptake of corona-coated NPs decreased as compared to pristine NPs while the highest cellular uptake of pristine NPs was associated with the

PVA-PEG-PLGA and PVA-D-PLGA in CHO-K1 cell line. On the other hand, the uptake of corona-coated NPs was elevated in PVA-D-PLGA as compared to other NPs in the CHO-K1 cell line. The highest FcR-mediated uptake of pristine and corona-coated NPs is demonstrated in Fig. 7b. The maximum cellular uptake of RAW264.7 cell line was related to the mid and small size ranges of PVA-PLGA and PVA-D-PLGA.
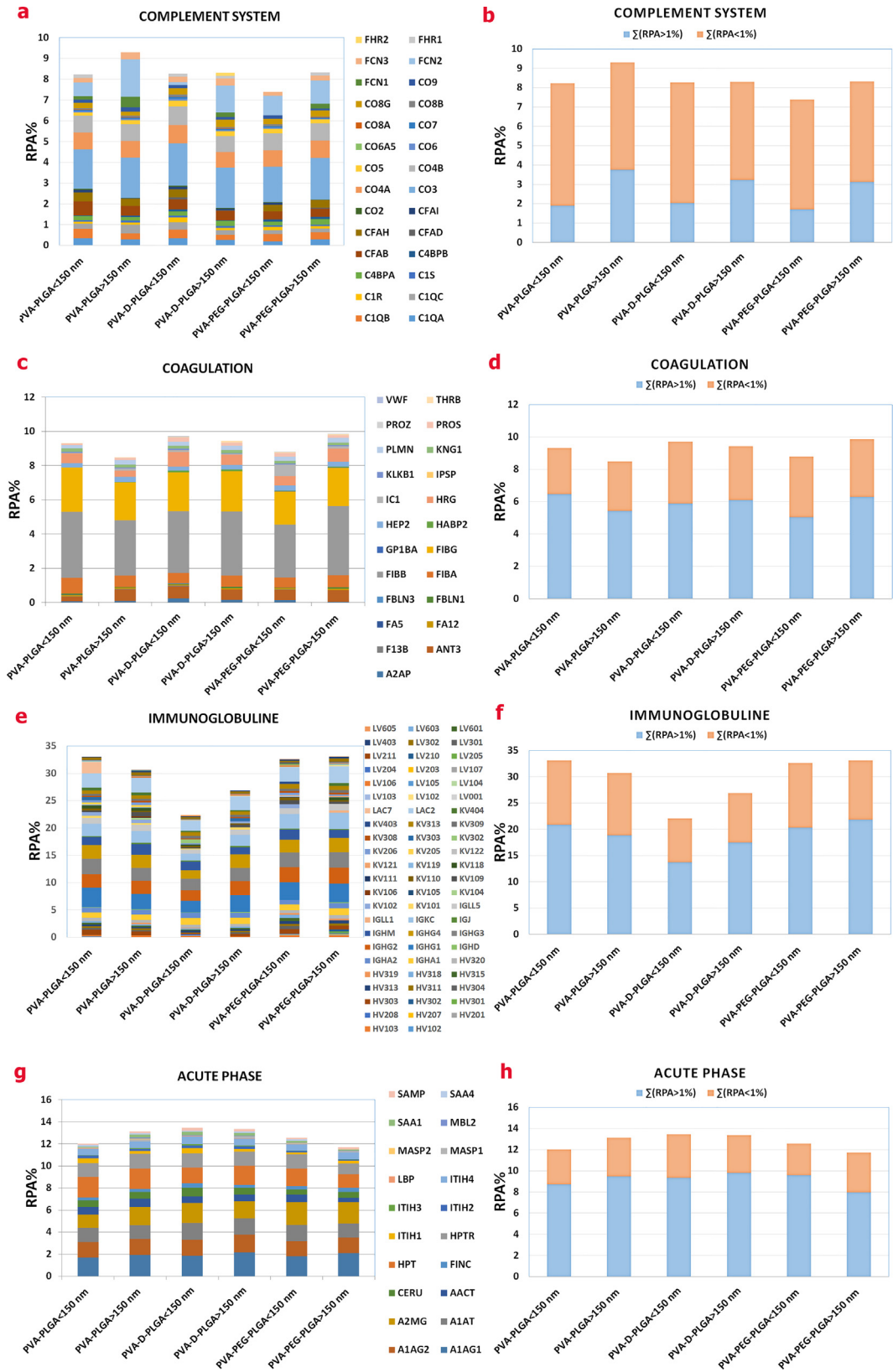
Fig. 4. Total percentage of identified proteins on the surface of PLGA-based NPs, classified based on functional protein groups (left panel) and abundance (right panel).
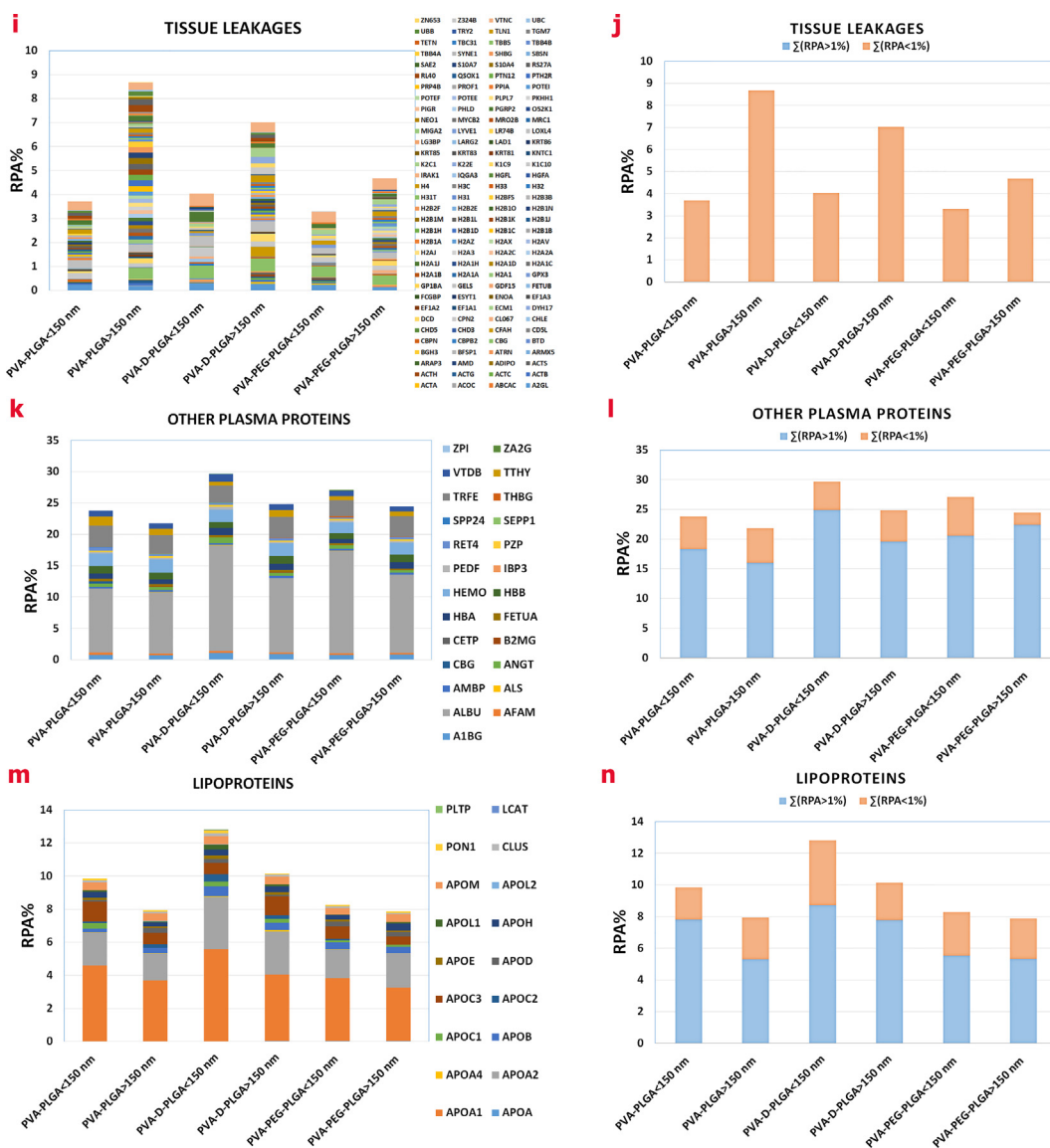
Fig. 4 (continued)

3.5. Correlation of FcR-mediated uptake and dysopsonins/opsonins ratio

The correlation between NP uptake intensity and the amount of opsonin proteins (immunoglobulins) adsorbed on the surface NPs is presented in Fig. 7c, d. It shows that the positive and negative correlations between dysopsonins and opsonins adsorbed on the surface NPs have an opposite trend with the amount of cellular uptake. The confocal images have been presented with respect to the maximum amounts of dysopsonins/opsonins ratio on the corona of NPs coated with PVA-D-PLGA (Fig. 8). NP- associated corona and pristine with higher adsorbed immunoglobulin content indicate that there is a greater uptake of NPs by RAW264.7 as compared to CHO-K1 cells. Dysopsonins/opsonins ratio in NPs with a size less than 150 nm as the maximum value between 0.8 and 1.4 reflects the lowest FcR-mediated uptake in macrophages.

4. Discussion

Most of the *in-vivo* and *in-vitro* investigations regarding polymeric NPs have been performed without considering the influence of man-made identity on protein-corona eventually affecting the NPs biological responses [28–31,33,34]. This study investigated the impacts of size, charge, and composition on adsorbed proteins on PLGA-based NPs. Further, *unique/common/similar* proteins were classified based on molecular weight and isoelectric point, and the effect of dysopsonins/opsonins ratio on NPs cellular uptake was determined for the first time. This was confirmed by our *in-vitro* data where the variation of *RPA* percentage of investigated NPs was associated to 10–20 kDa and 60–70 kDa molecular mass regions. Interestingly, the results of *RPA* under 100 kDa molecular mass were in accordance with the *RPA* results of liposomal [55] and inconsistent with inorganic NPs [43], respectively. The high relative abundance at 10–20 kDa and 60–70 kDa molecular masses belonged to the immunoglobulins and albumin, respectively, which could be defined for any polymeric NP with a peculiar synthetic identity. Significantly, immunological recognition occurs through the adsorption of immune-triggering proteins to the NPs surface as an opsonization process [58–60]. Several approaches have been well established for preventing and stimulating the opsonization of NPs [61–64]. The kinetics of protein adsorption are related to the composition of NPs while the variation in size
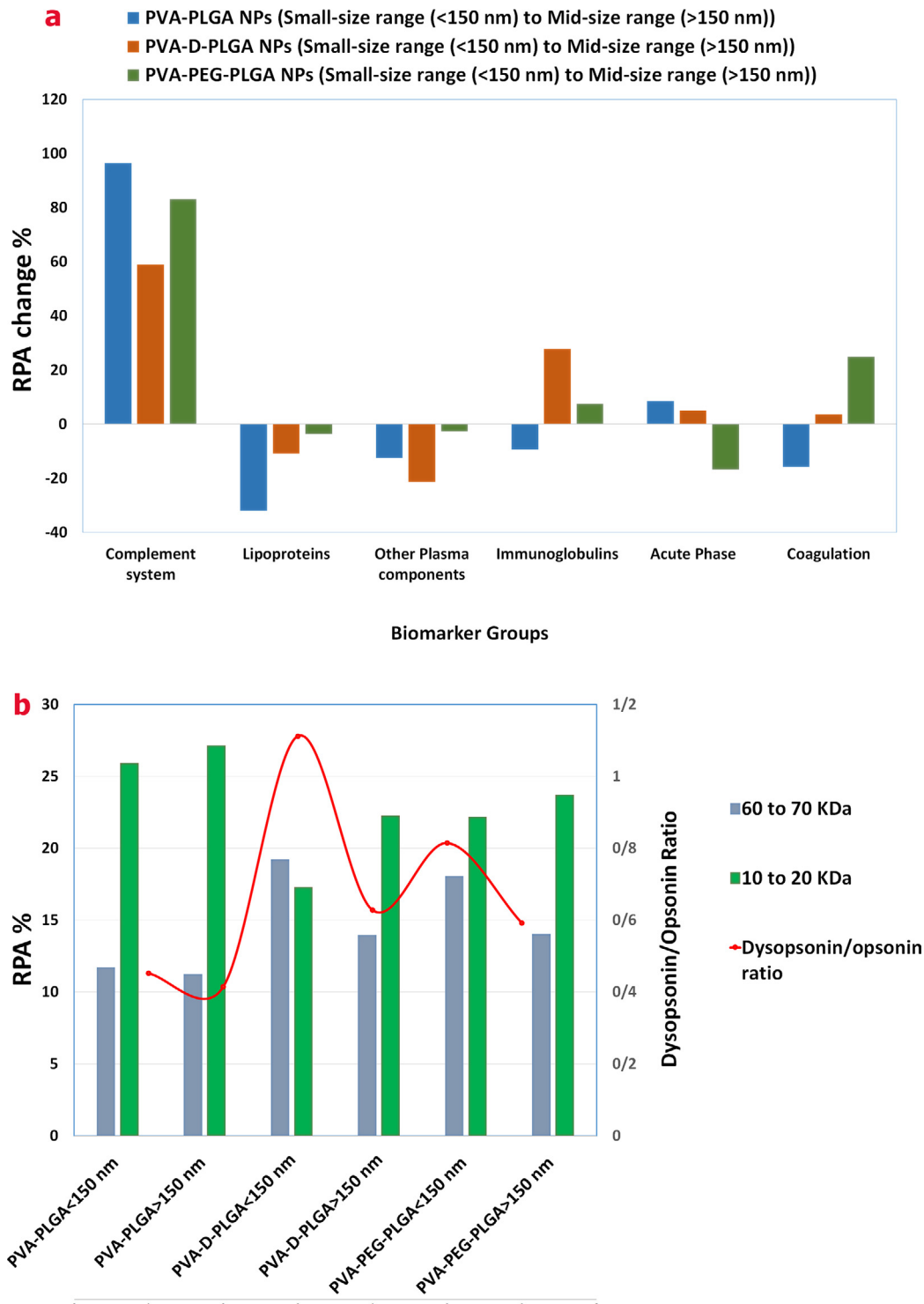
Fig. 5. The effect of NPs size on *RPA* changes percentage (a); Dysopsonin/opsonin ratio as *RPA* of two ranges of protein mass (b).

significantly affects the biological identity (similar/unique/common proteins) and the percentage of *RPA* of greater and less than 1% [13,65]. There is evidence of cross-relevance effects between particle size and surface chemistry on changes in the composition of the protein corona. In some cases, such effects are directly related to the intrinsic property of proteins, such as their shapes and physiological function [66,67]. It is already suggested that the safety of PLGA-based NPs in terms of cytotoxicity will seldom be influenced by the NPs surface modifications such as PVA or

DMAB coatings [30,35,37]. The development of NPs with hydrophilic properties using hydrophilic polymers such as polyvinyl alcohol and polyethylene glycol may promote the adsorption of albumin, fibrinogen and immunoglobulins [40]. Previously, it has been shown that the molecular weight of PEG and the density of PEG effectively enhance the fibrinogen adsorption [68] while in the current study, the relative abundance of fibrinogen increased by enlarging the size of PVA-PEG-PLGA NPs. Another factor affecting opsonization is the surface charge, which is considered as a
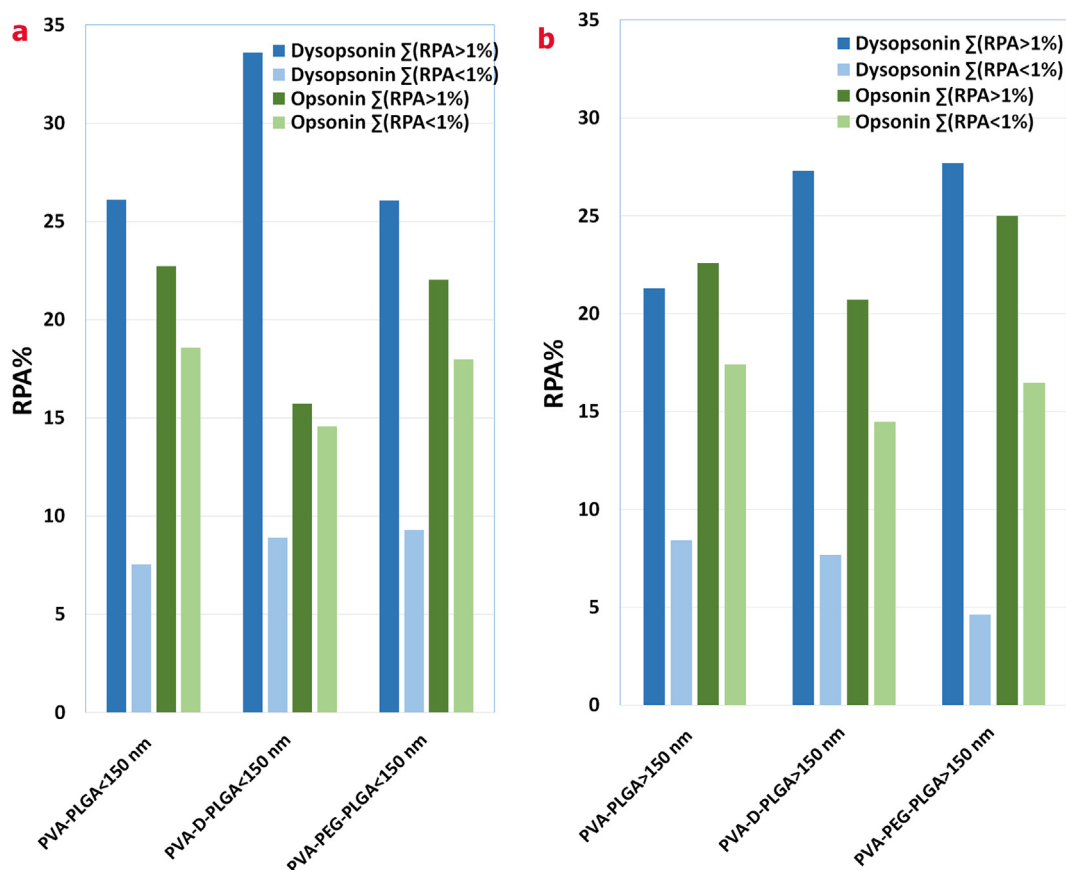
Fig. 6. *RPA* of dysopsonin and opsonins in less (a) and greater (b) than 150 nm identified on the surfaces of PLGA-based NPs; In panel (a), the *RPA* > 1% of dysopsonins adsorbed on PVA-ᴅ-PLGA NPs is higher than in the rest of the NPs. The percentage of opsonins abundance in PVA-ᴅ-PLGA NPs, greater and less than 1% is almost the same. In panel (b), the *RPA* > 1% and *RPA* < 1% of dysopsonins adsorbed on PVA-PLGA and PVA-PEG-PLGA NPs respectively have been less than in the rest of the NPs. The percentage of opsonins abundance in PVA-ᴅ-PLGA NPs (greater and less than 1%) is minimum.

determining factor which alters the fingerprint profile of protein corona [38,68,69]. Although the binding of the protein is affected by the surface charge of the particle [11,23], the reduction in the amount of immunoglobulins in the PVA-ᴅ-PLGA NPs is due to the DMAB-induced positive charge compared to other NPs. Further, the rise in the relative abundance percentage of complement proteins ($\sum RPA > 1\%$) in the investigated NPs was due to increased size of particles. Note that the effect of the size was previously evaluated on the quantity of proteins [23], while our results suggested that in addition to the NPs surface charge and composition, the effect of size dictates the type of adsorb unique proteins. Further, due to different surface charges of polymeric NPs, the adsorption of proteins might be partially dependent on the isoelectric point of proteins. This effect makes changes in the ratio of dysopsonins/opsonins as the surface charge of NPs governs the adsorption of proteins within the isoelectric point range of above and below 5.5.

Compared to the pristine NPs, corona-coated NPs indicated lower and different FcR-mediated uptake in comparison with FcR⁺ and FcR⁻ cells. The comparative correlation between the RAW264.7 [56] and CHO-K1 uptake as well the type of corona protein found in PLGA-based NPs, indicated that whatever the cell sees and reads (cell vision) is pertained to the amount and availability of rearranged protein motifs. Through interaction between immunoglobulins and the Fc receptor, the cells trigger the phagocytosis process [70,71]. In this regard, all corona-coated NPs were observed to have higher FcR-mediated uptake compared to the FcR⁻ cell line due to the interaction between immunoglobulins and Fc receptor on cells. Our findings suggest that the higher abun-

dance of dysopsonins, such as lipoprotein in PVA-ᴅ-PLGA NPs may cover the active sites of immunoglobulins causing a lower uptake [72]. On the other hand, the enhanced uptake of NPs with a higher immunoglobulin content is quantitatively confirmed by flow cytometry results. The high abundance of activated complement proteins in the corona may be due to their cleavage on the surfaces of corona coated NPs. In this case the lack of masking immunoglobulin active sites by C3 proteins and dysopsonins leads to existence of immunoglobulins in the corona layer interacting with Fc receptors of immune cells. According to the aforementioned statements, the high abundance of immunoglobulins in the protein corona is a necessary and sufficient condition for binding to the Fc receptor which could induce the uptake of NPs into macrophages. The correlation of the results with the relative abundance of immunoglobulins with the amount of macrophage uptake suggests that the precursor of the complement C3 proteins has been uncleavage in all PLGA-based NPs [73,74]. In addition to factors affecting surface chemistry and physicochemical properties, factors such as concentration, protein source, temperature, static or dynamic flow status could alter the protein corona profile, which was definite in our investigation. In this study, the total *RPA* below 1% was found to be between 35% and 40% of the total protein content of the protein corona. These low-abundant proteins interact with other proteins with a high amount of 1% affecting the biological identity of the NPs by modifying the dysopsonins/opsonins ratio. Ultimately, particular attention should be paid to the unique proteins with a high abundance of 1% (such as LAC7 in PVA-PLGA NPs), which affects the ratio of dysopsonins/opsonins, and it should be considered for future investigations.
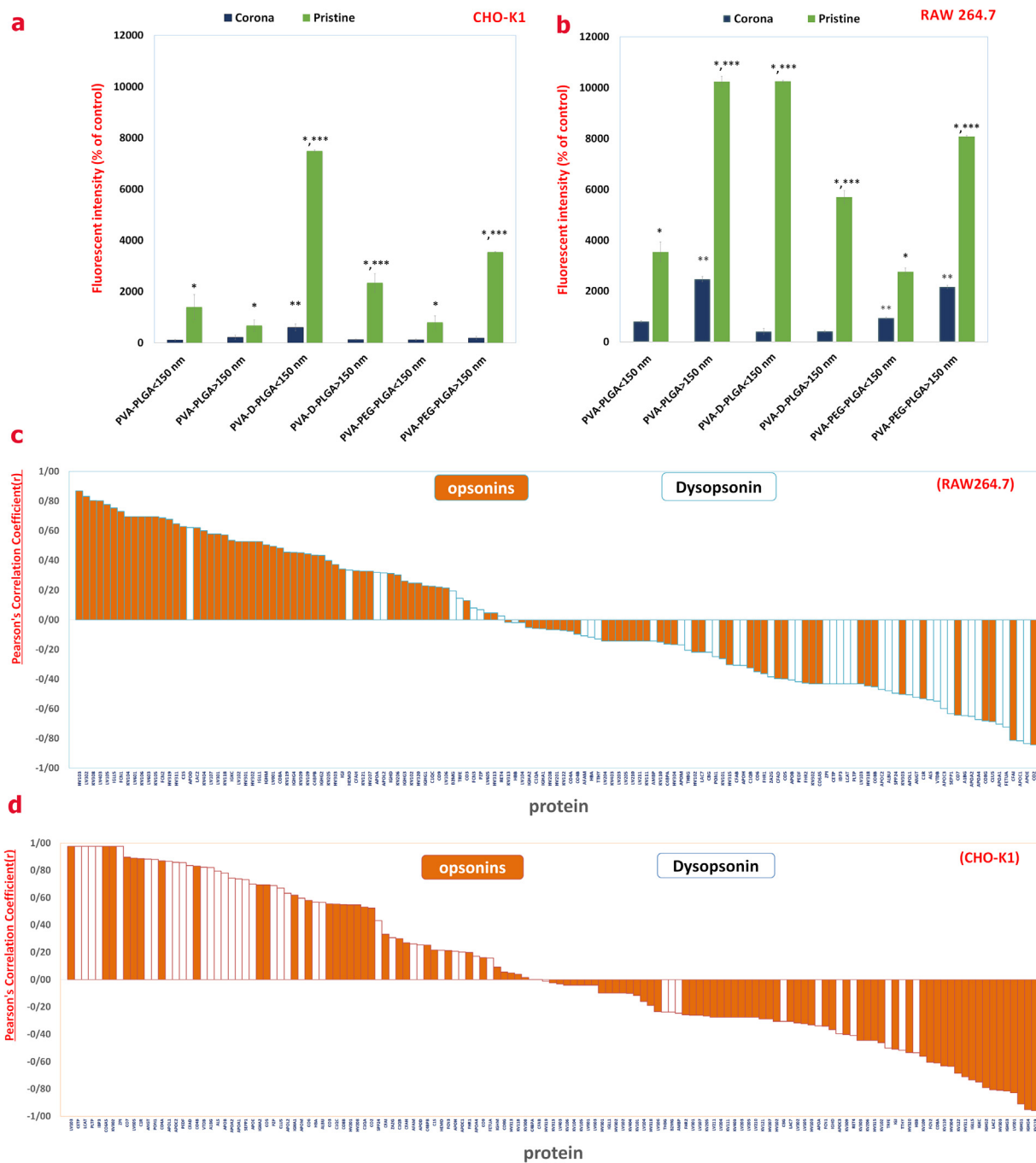
Fig. 7. Cellular uptake of pristine and corona-coated PLGA-based NPs in negative (a) and positive (b) Fc receptor cells; *: comparative uptake of analogous size pristine with corona-coated NPs; **: comparative uptake of corona coated NPs; ***: comparative uptake of pristine NPs; All data have been presented by one-way ANOVA and post hoc Tukey's test ($p < 0.01$). Comparative correlation between the RAW264.7 (c) and CHO-K1 (d) uptake and type of corona protein found in PLGA-based NPs in B$^+$ plasma condition; The dysopsonin and opsonin proteins have been highlighted based on FcR-mediated uptake indicating that the large positive or negative correlation in each cell has an opposite trend with each other.

5. Conclusion

In the current study, the fingerprint mapping of proteins adsorbed on the surface of PLGA-based NPs was reported considering the impact of NPs physicochemical properties on dysopsonins/opsonins ratio. This study demonstrated for the first time that the ratio of dysopsonins/opsonins was associated with the PLGA-based NPs possessing both positive and negative correlations related to the cellular uptake. This correlation for the cellular uptake was associated with the type of adsorbed proteins on NP surfaces as

well as the cell surface receptors. Opsonins provided positive and negative correlations in the uptake of corona coated NPs into the cells with (FcR$^+$) and without (FcR$^-$) expressed Fc receptor respectively. Thus, the spatial interactions of dysopsonins/opsonins proteins to each other could reveal the correlation between biological identity and the related immunological responses. Along with the identification of similar/unique and high-abundant proteins, the abundance of dysopsonins/opsonins ratio related to the 60–70 and 10–20 kDa regions on PLGA-based NPs can be inspiring for designing more efficient nano-systems. This study also
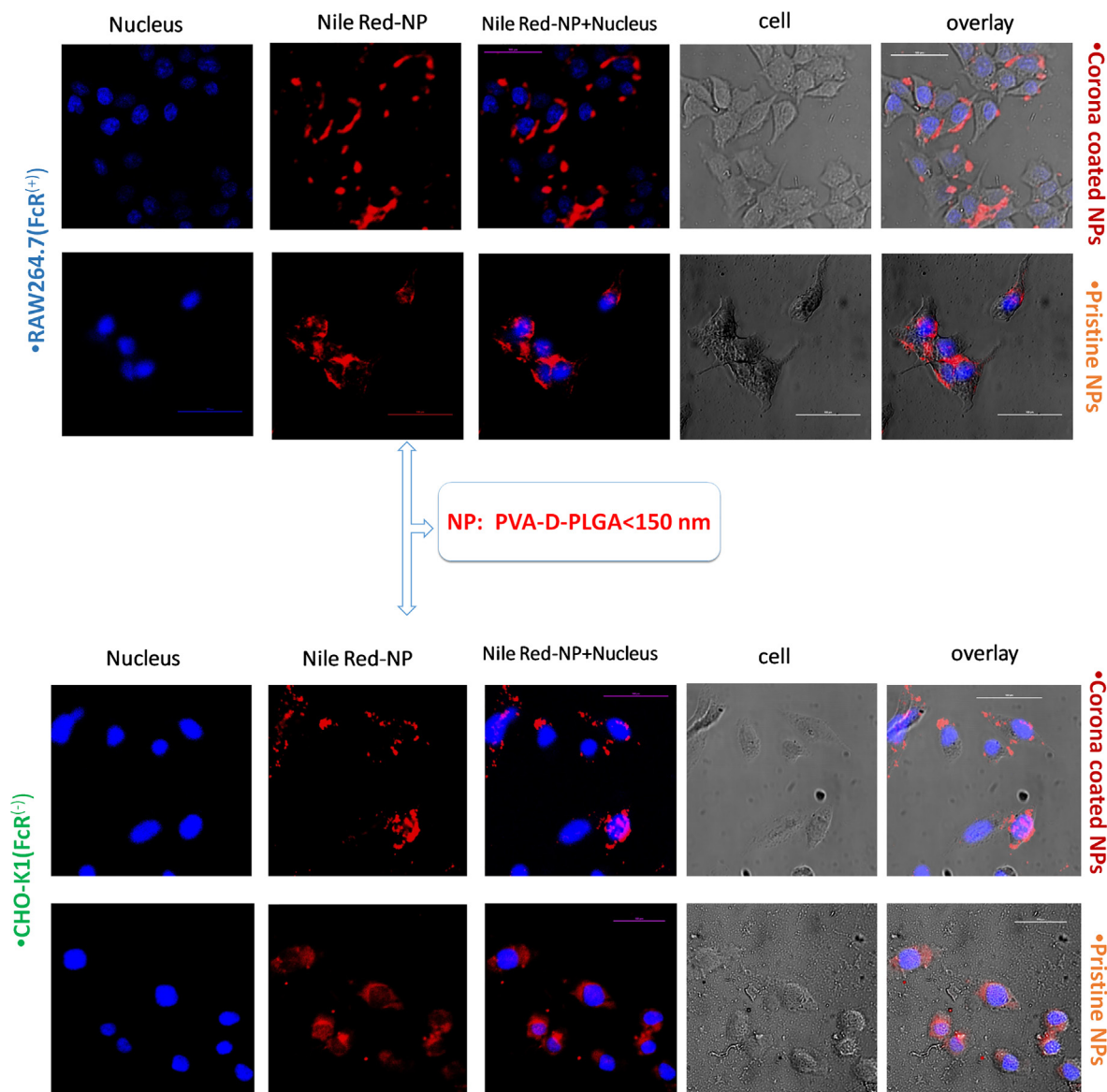
Fig. 8. Confocal images of RAW 264.7 and CHO-K1 cells incubated with nile red loaded pristine and corona-coated PVA-D-PLGA NPs (red) for 4 h, and labeled with DAPI (blue); FcR-mediated uptake of corona-coated NPs was higher for RAW264.7 compared to CHO-K1. Scale bars represent 100 μm.

provided guidelines for the correlation between physicochemical properties of NPs and dysopsonins/opsonins ratio leading to the conformational rearrangements that mitigate the challenge of NPs against immunological responses by the formation of protein corona.

CRediT authorship contribution statement

Ghassem Rezaei: Conceptualization, Data curation, Formal analysis, Investigation, Methodology, Software,Validation, Visualization, Writing – original draft, Writing – review & editing. **Seyed Mojtaba Daghighi:** Conceptualization, Data curation, Formal analysis, Methodology, Validation, Supervision, Visualization, Writing – original draft, Writing – review & editing. **Mohammad Raoufi:** Methodology, Software. **Mehdi Esfandyari-Manesh:** Investigation, Methodology, Formal analysis, Validation. **Mahban Rahimifard:** Investigation, Methodology, Formal analysis, Validation. **Vahid Iranpur Mobarakeh:** Investigation, Methodology, Formal analysis, Validation. **Sara Kamalzare:** Investigation, Methodology, Formal analysis, Validation. **Mohammad Hossein Ghahremani:** Method-

ology, Validation. **Fatemeh Atyabi:** Methodology, Validation, Visualization Writing – review & editing. **Mohammad Abdollahi:** Methodology, Validation, Visualization Writing – review & editing. **Farhad Rezaee:** Conceptualization, Data curation, Investigation, Formal analysis, Methodology, Validation, Visualization, Writing – review & editing. **Rassoul Dinarvand:** Conceptualization, Funding acquisition, Methodology, Project administration, Supervision, Validation, Visualization, Writing – review & editing

Declaration of Competing Interest

There are no conflicts of interest to declare.

Appendix A. Supplementary material

Detailed results of abundant proteins list and characterization data analyses are provided in Supplementary Information. Supplementary data to this article can be found online at https://doi.org/10.1016/j.jcis.2019.08.060.

References

[1] N. Kamaly, B. Yameen, J. Wu, O.C. Farokhzad, Degradable controlled-release polymers and polymeric nanoparticles: mechanisms of controlling drug release, Chem. Rev. 116 (4) (2016) 2602–2663.

[2] F. Mottaghitalab, M. Kiani, M. Farokhi, S.C. Kundu, R.L. Reis, M. Gholami, H. Bardania, R. Dinarvand, P. Geramifar, D. Beiki, Targeted delivery system based on gemcitabine-loaded silk fibroin nanoparticles for lung cancer therapy, ACS Appl. Mater. Interfaces 9 (37) (2017) 31600–31611.

[3] P. Couvreur, C. Vauthier, Nanotechnology: intelligent design to treat complex disease, Pharm. Res. 23 (7) (2006) 1417–1450.

[4] P. Mahdaviani, S. Bahadorikhalili, M. Navaei-Nigjeh, S.Y. Vafaei, M. Esfandyari-Manesh, A.H. Abdolghaffari, Z. Daman, F. Atyabi, M.H. Ghahremani, M. Amini, Peptide functionalized poly ethylene glycol-poly caprolactone nanomicelles for specific cabazitaxel delivery to metastatic breast cancer cells, Mater. Sci. Eng., C 80 (2017) 301–312.

[5] M. Mehdizadeh, H. Rouhani, N. Sepehri, R. Varshochian, M.H. Ghahremani, M. Amini, M. Gharghabi, S.N. Ostad, F. Atyabi, A. Baharian, Biotin decorated PLGA nanoparticles containing SN-38 designed for cancer therapy, Artif. Cells Nanomed. Biotechnol. 45 (3) (2017) 495–504.

[6] S. Sharma, A. Parmar, S. Kori, R. Sandhir, PLGA-based nanoparticles: a new paradigm in biomedical applications, TrAC, Trends Anal. Chem. 80 (2016) 30–40.

[7] M. Mahmoudi, A. Simchi, M. Imani, A.S. Milani, P. Stroeve, Optimal design and characterization of superparamagnetic iron oxide nanoparticles coated with polyvinyl alcohol for targeted delivery and imaging, J. Phys. Chem. B 112 (46) (2008) 14470–14481.

[8] R. Dinarvand, N. Sepehri, S. Manoochehri, H. Rouhani, F. Atyabi, Polylactide-co-glycolide nanoparticles for controlled delivery of anticancer agents, Int. J. Nanomed. 6 (2011) 877.

[9] M. Mahmoudi, N. Bertrand, H. Zope, O.C. Farokhzad, Emerging understanding of the protein corona at the nano-bio interfaces, Nano Today 11 (6) (2016) 817–832.

[10] C. Gunawan, M. Lim, C.P. Marquis, R. Amal, Nanoparticle–protein corona complexes govern the biological fates and functions of nanoparticles, J. Mater. Chem. B 2 (15) (2014) 2060–2083.

[11] M. Mahmoudi, I. Lynch, M.R. Ejtehadi, M.P. Monopoli, F.B. Bombelli, S. Laurent, Protein− nanoparticle interactions: opportunities and challenges, Chem. Rev. 111 (9) (2011) 5610–5637.

[12] C. Corbo, R. Molinaro, M. Tabatabaei, O.C. Farokhzad, M. Mahmoudi, Personalized protein corona on nanoparticles and its clinical implications, Biomater. Sci. 5 (3) (2017) 378–387.

[13] T. Cedervall, I. Lynch, S. Lindman, T. Berggård, E. Thulin, H. Nilsson, K.A. Dawson, S. Linse, Understanding the nanoparticle–protein corona using methods to quantify exchange rates and affinities of proteins for nanoparticles, Proc. Natl. Acad. Sci. 104 (7) (2007) 2050–2055.

[14] M. Mahmoudi, S. Laurent, M.A. Shokrgozar, M. Hosseinkhani, Toxicity evaluations of superparamagnetic iron oxide nanoparticles: cell "vision" versus physicochemical properties of nanoparticles, ACS Nano 5 (9) (2011) 7263–7276.

[15] M.P. Monopoli, D. Walczyk, A. Campbell, G. Elia, I. Lynch, F. Baldelli Bombelli, K.A. Dawson, Physical− chemical aspects of protein corona: relevance to in vitro and in vivo biological impacts of nanoparticles, J. Am. Chem. Soc. 133 (8) (2011) 2525–2534.

[16] S. Tenzer, D. Docter, S. Rosfa, A. Wlodarski, J.r. Kuharev, A. Rekik, S.K. Knauer, C. Bantz, T. Nawroth, C. Bier, Nanoparticle size is a critical physicochemical determinant of the human blood plasma corona: a comprehensive quantitative proteomic analysis, ACS Nano 5 (9) (2011) 7155–7167.

[17] H. Zhang, K.E. Burnum, M.L. Luna, B.O. Petritis, J.S. Kim, W.J. Qian, R.J. Moore, A. Heredia-Langner, B.J.M. Webb-Robertson, B.D. Thrall, Quantitative proteomics analysis of adsorbed plasma proteins classifies nanoparticles with different surface properties and size, Proteomics 11 (23) (2011) 4569–4577.

[18] E.A. Vogler, Protein adsorption in three dimensions, Biomaterials 33 (5) (2012) 1201–1237.

[19] C. Farrera, B. Fadeel, It takes two to tango: Understanding the interactions between engineered nanomaterials and the immune system, Eur. J. Pharm. Biopharm. 95 (2015) 3–12.

[20] K. Giri, K. Shameer, M.T. Zimmermann, S. Saha, P.K. Chakraborty, A. Sharma, R. R. Arvizo, B.J. Madden, D.J. Mccormick, J.-P.A. Kocher, Understanding protein–nanoparticle interaction: a new gateway to disease therapeutics, Bioconjug. Chem. 25 (6) (2014) 1078–1090.

[21] S. Tenzer, D. Docter, J. Kuharev, A. Musyanovych, V. Fetz, R. Hecht, F. Schlenk, D. Fischer, K. Kiouptsi, C. Reinhardt, Rapid formation of plasma protein corona critically affects nanoparticle pathophysiology, Nat. Nanotechnol. 8 (10) (2013) 772.

[22] U. Sakulkhu, M. Mahmoudi, L. Maurizi, G. Coullerez, M. Hofmann-Amtenbrink, M. Vries, M. Motazacker, F. Rezaee, H. Hofmann, Significance of surface charge and shell material of superparamagnetic iron oxide nanoparticle (SPION) based core/shell nanoparticles on the composition of the protein corona, Biomater. Sci. 3 (2) (2015) 265–278.

[23] P. Aggarwal, J.B. Hall, C.B. McLeland, M.A. Dobrovolskaia, S.E. McNeil, Nanoparticle interaction with plasma proteins as it relates to particle biodistribution, biocompatibility and therapeutic efficacy, Adv. Drug Deliv. Rev. 61 (6) (2009) 428–437.

[24] L. Ding, X. Zhu, Y. Wang, B. Shi, X. Ling, H. Chen, W. Nan, A. Barrett, Z. Guo, W. Tao, Intracellular fate of nanoparticles with polydopamine surface engineering and a novel strategy for exocytosis-inhibiting, lysosome impairment-based cancer therapy, Nano Lett. 17 (11) (2017) 6790–6801.

[25] X. Zhu, X. Ji, N. Kong, Y. Chen, M. Mahmoudi, X. Xu, L. Ding, W. Tao, T. Cai, Y. Li, Intracellular mechanistic understanding of 2D MoS2 nanosheets for anti-exocytosis-enhanced synergistic cancer therapy, ACS Nano 12 (3) (2018) 2922–2938.

[26] A. Albanese, P.S. Tang, W.C. Chan, The effect of nanoparticle size, shape, and surface chemistry on biological systems, Annu. Rev. Biomed. Eng. 14 (2012) 1–16.

[27] M. Mahmoudi, Protein corona: The golden gate to clinical applications of nanoparticles, 2016.

[28] A. Badkas, E. Frank, Z. Zhou, M. Jafari, H. Chandra, V. Sriram, J.-Y. Lee, J.S. Yadav, Modulation of in vitro phagocytic uptake and immunogenicity potential of modified Herceptin®-conjugated PLGA-PEG nanoparticles for drug delivery, Colloids Surf., B 162 (2018) 271–278.

[29] S. Xiong, X. Zhao, B.C. Heng, K.W. Ng, J.S.C. Loo, Cellular uptake of Poly-(D, L-lactide-co-glycolide)(PLGA) nanoparticles synthesized through solvent emulsion evaporation and nanoprecipitation method, Biotechnol. J. 6 (5) (2011) 501–508.

[30] S. Mura, H. Hillaireau, J. Nicolas, B. Le Droumaguet, S. Gueutin, S. Zanna, N. Tsapis, E. Fattal, Influence of surface charge on the potential toxicity of PLGA nanoparticles towards Calu-3 cells, Int. J. Nanomed. 6 (2011) 2591.

[31] H. Redhead, S. Davis, L. Illum, Drug delivery in poly (lactide-co-glycolide) nanoparticles surface modified with poloxamer 407 and poloxamine 908: in vitro characterisation and in vivo evaluation, J. Control. Release 70 (3) (2001) 353–363.

[32] Y. Thasneem, S. Sajeesh, C.P. Sharma, Glucosylated polymeric nanoparticles: a sweetened approach against blood compatibility paradox, Colloids Surf., B 108 (2013) 337–344.

[33] M.S. Cartiera, K.M. Johnson, V. Rajendran, M.J. Caplan, W.M. Saltzman, The uptake and intracellular fate of PLGA nanoparticles in epithelial cells, Biomaterials 30 (14) (2009) 2790–2798.

[34] K.Y. Win, S.-S. Feng, Effects of particle size and surface coating on cellular uptake of polymeric nanoparticles for oral delivery of anticancer drugs, Biomaterials 26 (15) (2005) 2713–2722.

[35] R. Gossmann, K. Langer, D. Mulac, New perspective in the formulation and characterization of Didodecyldimethylammonium Bromide (DMAB) stabilized poly (Lactic-co-Glycolic Acid)(PLGA) nanoparticles, PLoS ONE 10 (7) (2015) e0127532.

[36] D.E. Owens III, N.A. Peppas, Opsonization, biodistribution, and pharmacokinetics of polymeric nanoparticles, Int. J. Pharm. 307 (1) (2006) 93–102.

[37] F. Esmaeili, M.H. Ghahremani, B. Esmaeili, M.R. Khoshayand, F. Atyabi, R. Dinarvand, PLGA nanoparticles of different surface properties: preparation and evaluation of their body distribution, Int. J. Pharm. 349 (1–2) (2008) 249–255.

[38] R. Gossmann, E. Fahrländer, M. Hummel, D. Mulac, J. Brockmeyer, K. Langer, Comparative examination of adsorption of serum proteins on HSA-and PLGA-based nanoparticles using SDS–PAGE and LC–MS, Eur. J. Pharm. Biopharm. 93 (2015) 80–87.

[39] J. Shi, P.W. Kantoff, R. Wooster, O.C. Farokhzad, Cancer nanomedicine: progress, challenges and opportunities, Nat. Rev. Cancer 17 (1) (2017) 20.

[40] C.D. Walkey, W.C. Chan, Understanding and controlling the interaction of nanomaterials with proteins in a physiological environment, Chem. Soc. Rev. 41 (7) (2012) 2780–2799.

[41] J. Wolfram, Y. Yang, J. Shen, A. Moten, C. Chen, H. Shen, M. Ferrari, Y. Zhao, The nano-plasma interface: implications of the protein corona, Colloids Surf., B 124 (2014) 17–24.

[42] A. Gessner, A. Lieske, B.R. Paulke, R.H. Müller, Influence of surface charge density on protein adsorption on polymeric nanoparticles: analysis by two-dimensional electrophoresis, Eur. J. Pharm. Biopharm. 54 (2) (2002) 165–170.

[43] M.P. Monopoli, C. Åberg, A. Salvati, K.A. Dawson, Biomolecular coronas provide the biological identity of nanosized materials, Nat. Nanotechnol. 7 (12) (2012) 779.

[44] M. Lundqvist, J. Stigler, G. Elia, I. Lynch, T. Cedervall, K.A. Dawson, Nanoparticle size and surface properties determine the protein corona with possible implications for biological impacts, in: Proceedings of the National Academy of Sciences, 2008.

[45] V. Mirshafiee, M. Mahmoudi, K. Lou, J. Cheng, M.L. Kraft, Protein corona significantly reduces active targeting yield, Chem. Commun. 49 (25) (2013) 2557–2559.

[46] R.R. Arvizo, K. Giri, D. Moyano, O.R. Miranda, B. Madden, D.J. McCormick, R. Bhattacharya, V.M. Rotello, J.-P. Kocher, P. Mukherjee, Identifying new therapeutic targets via modulation of protein corona formation by engineered nanoparticles, PLoS ONE 7 (3) (2012) e33650.

[47] R.R. Arvizo, O.R. Miranda, D.F. Moyano, C.A. Walden, K. Giri, R. Bhattacharya, J. D. Robertson, V.M. Rotello, J.M. Reid, P. Mukherjee, Modulating pharmacokinetics, tumor uptake and biodistribution by engineered nanoparticles, PLoS ONE 6 (9) (2011) e24374.

[48] A.L. Capriotti, G. Caracciolo, G. Caruso, C. Cavaliere, D. Pozzi, R. Samperi, A. Laganà, Label-free quantitative analysis for studying the interactions between nanoparticles and plasma proteins, Anal. Bioanal. Chem. 405 (2–3) (2013) 635–645.

[49] W.-C. Shen, H. Ryser, Selective killing of Fc-receptor-bearing tumor cells through endocytosis of a drug-carrying immune complex, Proc. Natl. Acad. Sci. 81 (5) (1984) 1445–1447.

[50] U. Bilati, E. Allémann, E. Doelker, Development of a nanoprecipitation method intended for the entrapment of hydrophilic drugs into nanoparticles, Eur. J. Pharm. Sci. 24 (1) (2005) 67–75.

[51] K.C. Song, H.S. Lee, I.Y. Choung, K.I. Cho, Y. Ahn, E.J. Choi, The effect of type of organic phase solvents on the particle size of poly (d, l-lactide-co-glycolide) nanoparticles, Colloids Surf., A 276 (1–3) (2006) 162–167.

[52] F. Esmaeili, M.H. Ghahremani, S.N. Ostad, F. Atyabi, M. Seyedabadi, M.R. Malekshahi, M. Amini, R. Dinarvand, Folate-receptor-targeted delivery of docetaxel nanoparticles prepared by PLGA–PEG–folate conjugate, J. Drug Target. 16 (5) (2008) 415–423.

[53] H. Fasehee, R. Dinarvand, A. Ghavamzadeh, M. Esfandyari-Manesh, H. Moradian, S. Faghihi, S.H. Ghaffari, Delivery of disulfiram into breast cancer cells using folate-receptor-targeted PLGA-PEG nanoparticles: in vitro and in vivo investigations, J. Nanobiotechnol. 14 (1) (2016) 32.

[54] M. Yang, S.K. Lai, T. Yu, Y.-Y. Wang, C. Happe, W. Zhong, M. Zhang, A. Anonuevo, C. Fridley, A. Hung, Nanoparticle penetration of human cervicovaginal mucus: The effect of polyvinyl alcohol, J. Control. Release 192 (2014) 202–208.

[55] D. Pozzi, G. Caracciolo, A.L. Capriotti, C. Cavaliere, G. La Barbera, T.J. Anchordoquy, A. Laganà, Surface chemistry and serum type both determine the nanoparticle–protein corona, J. Proteomics 119 (2015) 209–217.

[56] K. Saha, M. Rahimi, M. Yazdani, S.T. Kim, D.F. Moyano, S. Hou, R. Das, R. Mout, F. Rezaee, M. Mahmoudi, Regulation of macrophage recognition through the interplay of nanoparticle surface functionality and protein corona, ACS Nano 10 (4) (2016) 4421–4430.

[57] R. Zucker, K. Daniel, E. Massaro, S. Karafas, L. Degn, W. Boyes, Detection of silver nanoparticles in cells by flow cytometry using light scatter and far-red fluorescence, Cytometry Part A 83 (10) (2013) 962–972.

[58] H.S. Goodridge, D.M. Underhill, N. Touret, Mechanisms of Fc receptor and dectin-1 activation for phagocytosis, Traffic 13 (8) (2012) 1062–1071.

[59] S. Nagayama, K.-I. Ogawara, Y. Fukuoka, K. Higaki, T. Kimura, Time-dependent changes in opsonin amount associated on nanoparticles alter their hepatic uptake characteristics, Int. J. Pharm. 342 (1–2) (2007) 215–221.

[60] J.-C. Leroux, F. De Jaeghere, B. Anner, E. Doelker, R. Gurny, An investigation on the role of plasma and serum opsonins on the internalization of biodegradable poly (D, L-lactic acid) nanoparticles by human monocytes, Life Sci. 57 (7) (1995) 695–704.

[61] F. Danhier, N. Lecouturier, B. Vroman, C. Jérôme, J. Marchand-Brynaert, O. Feron, V. Préat, Paclitaxel-loaded PEGylated PLGA-based nanoparticles: in vitro and in vivo evaluation, J. Control. Release 133 (1) (2009) 11–17.

[62] R. Safavi-Sohi, S. Maghari, M. Raoufi, S.A. Jalali, M.J. Hajipour, A. Ghassempour, M. Mahmoudi, Bypassing protein corona issue on active targeting: zwitterionic coatings dictate specific interactions of targeting moieties and cell receptors, ACS Appl. Mater. Interfaces 8 (35) (2016) 22808–22818.

[63] E.V. Potter, G.H. Stollerman, The opsonization of bentonite particles by γ-globulin, J. Immunol. 87 (1) (1961) 110–118.

[64] M.W. Rytel, G.H. Stollerman, The opsonic effect of complement on the phagocytosis of γ-globulin-coated bentonite particles, J. Immunol. 90 (4) (1963) 607–611.

[65] C. Ge, J. Du, L. Zhao, L. Wang, Y. Liu, D. Li, Y. Yang, R. Zhou, Y. Zhao, Z. Chai, Binding of blood proteins to carbon nanotubes reduces cytotoxicity, Proceedings of the National Academy of Sciences, 2011.

[66] S.T. Yang, Y. Liu, Y.W. Wang, A. Cao, Biosafety and bioapplication of nanomaterials by designing protein–nanoparticle interactions, Small 9 (9–10) (2013) 1635–1653.

[67] J.H. Shannahan, X. Lai, P.C. Ke, R. Podila, J.M. Brown, F.A. Witzmann, Silver nanoparticle protein corona composition in cell culture media, PLoS ONE 8 (9) (2013) e74001.

[68] M. Ferrari, Frontiers in cancer nanomedicine: directing mass transport through biological barriers, Trends Biotechnol. 28 (4) (2010) 181–188.

[69] K. Sempf, T. Arrey, S. Gelperina, T. Schorge, B. Meyer, M. Karas, J. Kreuter, Adsorption of plasma proteins on uncoated PLGA nanoparticles, Eur. J. Pharm. Biopharm. 85 (1) (2013) 53–60.

[70] A. Sobota, A. Strzelecka-Kiliszek, E. Gładkowska, K. Yoshida, K. Mrozińska, K. Kwiatkowska, Binding of IgG-opsonized particles to FcγR is an active stage of phagocytosis that involves receptor clustering and phosphorylation, J. Immunol. 175 (7) (2005) 4450–4457.

[71] P. Pacheco, D. White, T. Sulchek, Effects of microparticle size and Fc density on macrophage phagocytosis, PLoS ONE 8 (4) (2013) e60989.

[72] V. Mirshafiee, R. Kim, S. Park, M. Mahmoudi, M.L. Kraft, Impact of protein pre-coating on the protein corona composition and nanoparticle cellular uptake, Biomaterials 75 (2016) 295–304.

[73] E.J. Brown, Complement receptors and phagocytosis, Curr. Opin. Immunol. 3 (1) (1991) 76–82.

[74] K.P. van Kessel, J. Bestebroer, J.A. van Strijp, Neutrophil-mediated phagocytosis of Staphylococcus aureus, Front. Immunol. 5 (2014) 467.